Open Access Online Journal on Astronomy and Astrophysics

Acta Astrophysica Taurica

www.astrophysicatauricum.org

Acta Astrophys. Tau. 5(1), 11–20 (2024)

doi:10.34898/aat.vol5.iss1.pp11-20

Transverse component of the longitudinal magnetic field gradient in active regions with different levels of flare productivity: different approaches to calculation, dynamics and probable critical values

Yu.A. Fursyak

Crimean Astrophysical Observatory, Nauchny 298409
e-mail: yuriy_fursyak@mail.ru

Received 4 October 2022

ABSTRACT

This study aims to analyze the value and dynamics of the transverse component of the longitudinal magnetic field gradient in active regions (ARs) with different levels of flare productivity. We use magnetographic data from the Helioseismic and Magnetic Imager (HMI) instrument onboard the Solar Dynamics Observatory (SDO) on the spatial distribution of the B_z component of the magnetic field vector at the solar photospheric level. Thirteen ARs were selected for analysis: 6 ARs with low activity and 7 ARs with high activity; two of them are ARs with an additional emergence of the magnetic flux. Monitoring of each of the ARs was carried out for 3–5 days within 30–35 heliographic degrees relative to the central meridian. Two approaches to calculating the longitudinal magnetic field gradient are considered: modern, which requires the magnetographic data of high spatial resolution, and classical. For each approach, the parameters characterizing the longitudinal magnetic field gradient in the AR were determined. For the modern approach, this is the average value of the transverse component of the longitudinal magnetic field gradient $< \nabla_\perp B_z >$ over the AR; for the classical approach, this is the maximum value of the transverse component of the longitudinal magnetic field gradient for a set of the pairs of sunspots in the AR ($max(\nabla_\perp B_z)$). The dynamics of the chosen parameters was compared with the level of AR flare productivity. It is shown that: (1) There are threshold values of the parameters that describe the longitudinal magnetic field gradient of the AR. For $< \nabla_\perp B_z >$ the critical value is 0.08 Gs km^{-1}, and for the parameter $max(\nabla_\perp B_z)$ it is 0.115 Gs km^{-1}. (2) The first powerful flares of X-ray class M or higher are observed in the AR 23–25 hours after the above parameters exceed the corresponding critical values.

Key words: Sun, magnetic fields, active regions, solar activity

1 Introduction

Studying the magnetic fields on the Sun and their dynamics is the first and undoubtedly crucial step in understanding active processes and phenomena observed in the solar atmosphere.

The world's first measurements of sunspot magnetic fields were carried out by Hale (1908) using the spectrographic data from the solar tower telescope at the Mount Wilson Observatory. There was further a need to measure even weaker local magnetic fields. However, the initial attempts of such measurements using photoelectric methods by G.E. Hale and colleagues in 1933 were unsuccessful.

Technological advancements led to the emergence of solar magnetographs in the 1950s and their further development. The first magnetograph was developed in 1952 by Babcock (1953). A few years later, a similar device was mounted on the solar tower telescope at the Crimean Astrophysical Observatory (Nikulin et al., 1958), and by the mid-1960s, magnetographs were being used in many major observatories and institutes involved in studying the Sun, such as IZMIRAN (Ioshpa, Obridko, 1965), Pulkovo Observatory (Ikhsanov, Platonov, 1967), SibIZMIR (Kuznetsov et al., 1966), Climax Observatory (Lee et al., 1965), Kitt Peak Observatory (Livingston, 1968), etc.

The advent of the first magnetographs laid the foundation for the systematic study of magnetic fields in the solar atmosphere. By the late 1950s, based on a significant amount of observational data, a conclusion was drawn on the close connection between magnetic fields and non-stationary processes in the solar atmosphere (Severnyi, 1956, 1957, and others). As noted by A.B. Severny, even "a basic consideration of energy balance shows that there is no other source of energy for solar flares inside the solar atmosphere except for magnetic energy" (Severnyi, 1988). Researchers determine parameters of the magnetic field that can be estimated without invoking complex mathematical calculations but meanwhile easily linked to the dynamics of flare productivity in the AR. The simplest of such quantities are the magnetic field strength of sunspots in a group, complexity of the magnetic configuration, magnetic flux, and some others. A more complex

parameter is the magnetic field gradient. Here, we are only referring to the transverse component of the longitudinal magnetic field since even today there are significant challenges in measuring magnetic fields at two or more heights in the solar atmosphere. Although thanks to introducing multichannel vector magnetographs (e.g., Bruns et al., 1965; Nikulin, 1967), such studies have been carried out in the past, but only a small number of them contain information on the values of the vertical component of the longitudinal magnetic field gradient (Kotov, 1970; Baranovskii, Stepanov, 1959; Houtgast, Sluiters, 1948). There are also theoretical studies (see, e.g., Leroy, 1962; Severnyi, 1965; Ioshpa, Mogilevskii, 1965) in which data on the vertical component of the longitudinal magnetic field gradient were obtained from the equation $div\vec{B} = 0$. However, there is no systematic studies on sufficiently large statistical material in this direction at all.

By the end of the 1950s, a group of Crimean astronomers led by A.B. Severny studied the transverse gradients of the longitudinal magnetic field and their dynamics before and after solar flares. Significant results were obtained. For instance, in Severnyi (1958) it was noted that "flares occur at neutral points (regions) of the magnetic field of sunspot groups with a significant field gradient near these points". In 1959, a statistical analysis was conducted based on accumulated observational data, revealing that powerful flare processes occur in areas with a longitudinal magnetic field gradient exceeding 0.1 Gs km^{-1} (Severnyi, 1960). These findings were further confirmed in a series of studies (Gopasyuk et al., 1963; Zvereva, Severnyi, 1970, and others). The close connection between high field gradients and powerful eruptive events in the solar atmosphere was also identified based on observations from other observatories, such as the Medon Observatory (Avignon et al., 1964; Caroubalos, 1964). Here, instead of gradients, the ratio d/D was used, where d is the distance between sunspots and D is the diameter of the larger sunspot. By the late 1970s, the threshold value of the longitudinal magnetic field gradient, 0.1 Gs km^{-1}, was established by Soviet astronomers as one of the parameters enabling an accurate (with over 80% reliability) forecast of AR flare productivity with a lead time of 1–3 days (Severny et al., 1979; Altyntsev et al., 1982).

In recent decades, instruments for measuring magnetic fields on the Sun, particularly those mounted on spacecrafts, have numerous advantages over earlier magnetographs. These advantages include the ability to make a full-time monitoring of the Sun with high spatial and temporal resolution. For example, the resolving power of the Babcock magnetograph was approximately $38'' \times 70''$, whereas that of the Crimean Astrophysical Observatory magnetograph was $15'' \times 30''$ (about 11000×22000 km at the level of the solar photosphere). In contrast, the Helioseismic and Magnetic Imager (HMI, Scherrer et al., 2012) onboard the Solar Dynamics Observatory (SDO, Pesnell et al., 2012) has a spatial resolution at the solar photospheric level of about $0.5''$ ($\approx$360 km), while the spectropolarimeter SOT-SP/Hinode (Kosugi et al., 2007) has a resolution of about $0.3''$ ($\approx$220 km).

Taking into account the advantages of modern instruments for studying the Sun, it would be interesting to repeat early research in analyzing the structure and dynamics of longitudinal magnetic field gradients. This paper aims to study the dynamics of the transverse component of the longitudinal magnetic field gradient on the basis of a relatively small representative sample of ARs with varying levels of flare productivity and to determine threshold values of the gradient, comparing them with the previously found value of 0.1 Gs km^{-1}.

2 Observational data

The main part of work was carried out using data from the HMI/SDO instrument, which are available on the Joint Science Operation Center (JSOC) website[1]. SHARP (Spaceweather HMI Active Region Patch) (Bobra et al., 2014) magnetograms of the spatial distribution of the vertical component (B_z) of the magnetic field vector in the photosphere were used (cylindrical coordinates, data series hmi.sharp_cea_720s) with a temporal resolution of 12 minutes.

We also used data from the GOES-15[2] weather monitoring satellite regarding the X-ray flux in the 1–8 Å wavelength range at the Earth orbit, as well as information on the parameters of ARs and flares in them, published on the website of the Laboratory of Solar Astronomy of Space Research Institute and the Institute of Solar-Terrestrial Physics[3].

Thirteen ARs from solar activity cycle 24, which have different levels of flare productivity, were selected for analysis. Note that by an active region we mean a group of sunspots. The analyzed regions were divided into three groups. Regions with low activity (hereafter AR activity should be understood as flare activity) are characterized by flares of X-ray class C or M not exceeding M5.0. A total of 6 such regions were analyzed. Regions with high activity (5 ARs analyzed) are characterized by a series of flares of X-ray class M5.0 and higher or one or more flares of X-ray class X. The third group (two ARs) includes regions with high activity in which a significant increase of the magnetic flux was observed during monitoring (5 times or more).

The main information on the studied ARs is presented in Table 1. It includes the NOAA classification number (second column of the table), the monitoring time for each region (third column). To minimize errors in calculating the magnetic field gradient, caused by the projection effect, the monitoring time for each region was limited to the time interval within $\pm 35°$ relative to the central solar meridian (3–5 days). The fourth column of the table indicates the X-ray class and the date of the most powerful flare recorded in the analyzed region during its presence on the visible solar disk. The fifth column represents the flare index (FI, Abramenko, 2005) of the AR – a parameter characterizing the flare productivity of ARs. The flare index is equal to 1.0 (100.0) if one flare of X-ray class C1.0 (X1.0) occurs daily in the AR during its visibility on the solar disk. The FI value is calculated for the entire time the AR is visible on the solar disk. The last two columns of the table contain information on the values of parameters of the transverse component of the longitudinal magnetic field gradient in the studied ARs – the average

[1] http://jsoc2.stanford.edu/ajax/lookdata.html
[2] https://satdat.ngdc.noaa.gov/sem/goes/data/full
[3] https://tesis.xras.ru

Table 1. Information on the studied active regions, their flare activity, and values of the transverse component of the longitudinal magnetic field gradient

No.	Region Number (NOAA)	Monitoring Time	Most Powerful Flare in the AR	FI	$< \overline{\nabla_\perp B_z} >$, Gs km^{-1}	$\overline{max(\nabla_\perp B_z)}$, Gs km^{-1}
1	**2**	**3**	**4**	**5**	**6**	**7**
Regions with Low Activity						
1	11391	07.01.2012 – 10.01.2012	C2.2 13.01.2012	0.30	0.090	0.084
2	11899	17.11.2013 – 20.11.2013	M1.1 23.11.2013	3.85	0.070	0.004
3	12381	07.07.2015 – 10.07.2015	M1.7 06.07.2015	5.25	0.088	0.088
4	12480	10.01.2016 – 14.01.2016	C1.7 15.01.2016	0.23	0.073	0.013
5	12494	05.02.2016 – 07.02.2016	C5.2 04.02.2016	1.77	0.084	0.095
6	12674	03.09.2017 – 06.09.2017	C5.2 30.08.2017	0.76	0.093	0.112
Regions with High Activity						
7	11283	04.09.2011 – 07.09.2011	X2.1 06.09.2011	45.61	0.087	0.206
8	11890	07.11.2013 – 10.11.2013	X3.3 05.11.2013	55.63	0.096	0.631
9	12158	09.09.2014 – 12.09.2014	X1.6 10.09.2014	13.00	0.095	0.118
10	12192	22.10.2014 – 25.10.2014	X3.1 25.10.2014	101.64	0.120	0.335
11	12297	11.03.2015 – 14.03.2015	X2.2 11.03.2015	46.32	0.095	0.792
Regions with Additional Magnetic Flux Emergence						
12	11158	12.02.2011 – 15.02.2011	X2.2 15.02.2011	59.26	0.105	0.331
13	12673	02.09.2017 – 05.09.2017	X9.3 06.09.2017	223.86	0.102	0.476

value of the transverse component of the longitudinal magnetic field gradient over the monitoring time (averaging over time denoted by the horizontal line on top; sixth column) and the average value of the maximum transverse component of the longitudinal magnetic field gradient between sunspot pairs in the AR over the monitoring time (seventh column). More detailed information on these parameters will be provided below in Section 3.

All the ARs presented in Table 1 are divided into three subgroups: regions with low flare activity, regions with high activity, and regions with additional emergence of the magnetic flux. In each subgroup of the table, the ARs are arranged in chronological order.

3 Results

3.1 First approach to calculating the transverse component of the longitudinal magnetic field gradient: features and key findings

The first approach to calculating the transverse component of the longitudinal magnetic field gradient (denoted as $\nabla_\perp B_z$) is modern. To implement this approach, it is required to use high spatial resolution magnetographic data of the distribution of the vertical component (B_z) of the magnetic field vector at a specified level of the solar atmosphere. The standard formula adopted to calculate the field gradient

$$< \nabla_\perp B_z >= \sqrt{(\frac{\partial B_z}{\partial x})^2 + (\frac{\partial B_z}{\partial y})^2}. \quad (1)$$

The derivatives $\frac{\partial B_z}{\partial x}$ and $\frac{\partial B_z}{\partial y}$ were calculated using approximate calculation formulas. Here, the following formula for calculating the derivative using five points (pixels on the magnetogram) is applied:

$$f'(x_0) \approx \frac{-f(x_0+2h)+8f(x_0+h)-8f(x_0-h)+f(x_0-2h)}{12h}, \quad (2)$$

where x_0 is the pixel at which the derivative value needs to be calculated and h is the step of differentiation, equal to the pixel size on the magnetogram in our case. The magnetic field gradient value is calculated in Gs km^{-1}. Note that the choice of a five-point (five-pixel) differentiation window is not random and represents a certain compromise: when differentiating using a small number of points, the results obtained will be highly noisy, and when differentiating using a large number of points, some significant information will be lost.

The implementation of the first approach allows for the construction of a detailed map showing the distribution of $\nabla_\perp B_z$ at a specified level of the solar atmosphere. An example of such a map, computed based on spatial distribution data of the B_z component of the magnetic field at the solar photospheric level, is presented in Fig. 1. The white bold curve in Fig. 1 denotes the boundaries of the AR (standard bitmap masking provided along with the HMI/SDO magnetogram data package) on the rectangular SHARP magnetogram. The parameters of $\nabla_\perp B_z$ were calculated only for the pixels located inside the white bold curve.

Note that the maps of the longitudinal magnetic field gradient similar to that presented in Fig. 1 were previously accessible on the website solarmonitor.org (Fig. 2). These data were provided by the GONG (Global Oscillation Network Group) telescope network. However, since mid-2011, information on the longitudinal magnetic field gradient has become unavailable on this website.

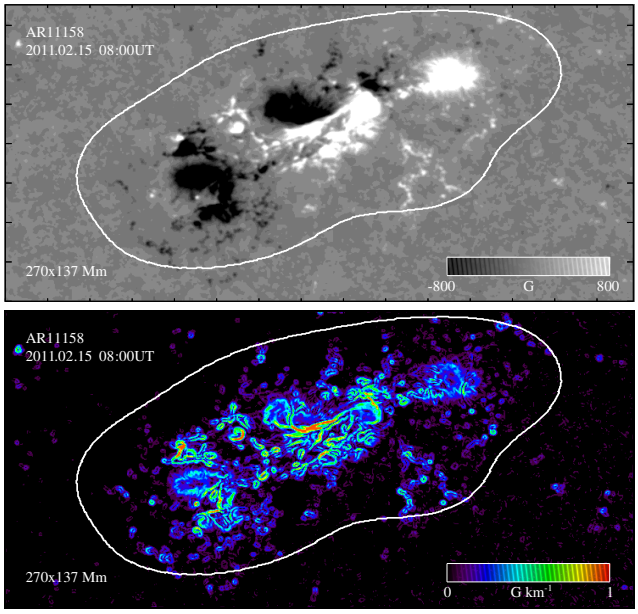

Fig. 1. Top panel: a map showing the distribution of the vertical component (B_z) of the magnetic field vector at the level of the solar photosphere (HMI/SDO data) for NOAA AR 11158 at 08:00 UT on 15 February 2011; bottom panel: a map constructed based on it showing the spatial distribution of the transverse component of the longitudinal magnetic field gradient $\nabla_\perp B_z$.

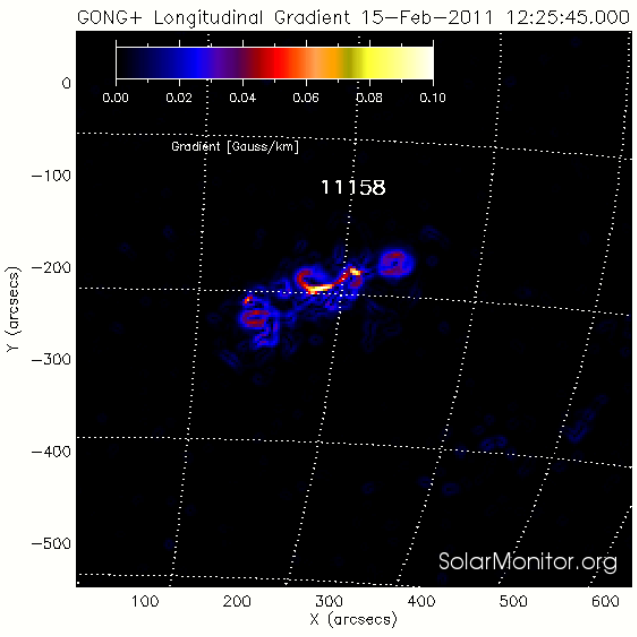

Fig. 2. Map of the spatial distribution of the longitudinal magnetic field gradient in NOAA AR 11158 at 12:45 UT on 15 February 2011, calculated based on data from the GONG telescope network and available on the website solarmonitor.org

The average value of the transverse component of the longitudinal magnetic field gradient $< \nabla_\perp B_z >$ for the AR was

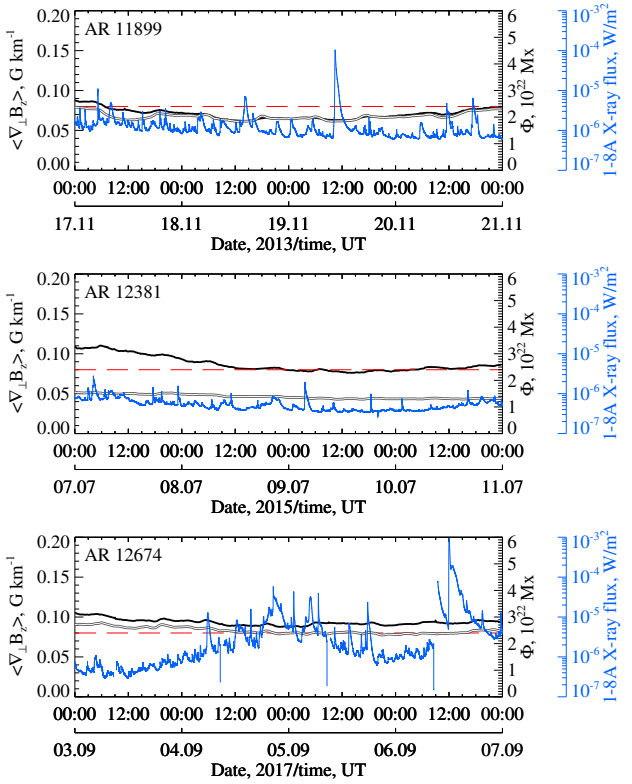

Fig. 3. Dynamics of the magnetic flux (gray double curve), average value of the transverse component of the longitudinal magnetic field gradient $< \nabla_\perp B_z >$ (black curve), and X-ray flux in the wavelength range of 1–8 Å at the Earth orbit (blue curve) for three regions with low flare activity from the analyzed sample. The critical level of $< \nabla_\perp B_z >$ is indicated by the red long-dashed line (for more details, see the text).

chosen as the basic parameter describing the longitudinal magnetic field gradient. This parameter was calculated for each AR in the analyzed sample and for each magnetogram during the monitoring period. The temporal variations of $< \nabla_\perp B_z >$ were compared in each case with the flare productivity dynamics of the AR. Several typical graphs are presented in Figs. 3 and 4. Figure 3 shows the dynamics of $< \nabla_\perp B_z >$ for three ARs with low activity, while Fig. 4 shows three ARs with high activity. The graphs also illustrate the magnetic flux dynamics (gray double curve) and data from the GOES-15 spacecraft on the X-ray flux in the 1–8 Å wavelength range at the Earth orbit (blue curve). The X-ray classes of the most powerful flares (higher than X5.0 class), associated with the studied AR during its monitoring period, are indicated.

From the graphs presented in Figs. 3 and 4 we can see the following:

1. The value of $< \nabla_\perp B_z >$ shows an insignificant spread for ARs from the analyzed sample. Based on the data provided in the sixth column of Table 1, which lists the average values of the transverse component of the longitudinal magnetic field gradient $< \overline{\nabla_\perp B_z} >$ over the monitoring period, it can be seen that the maximum

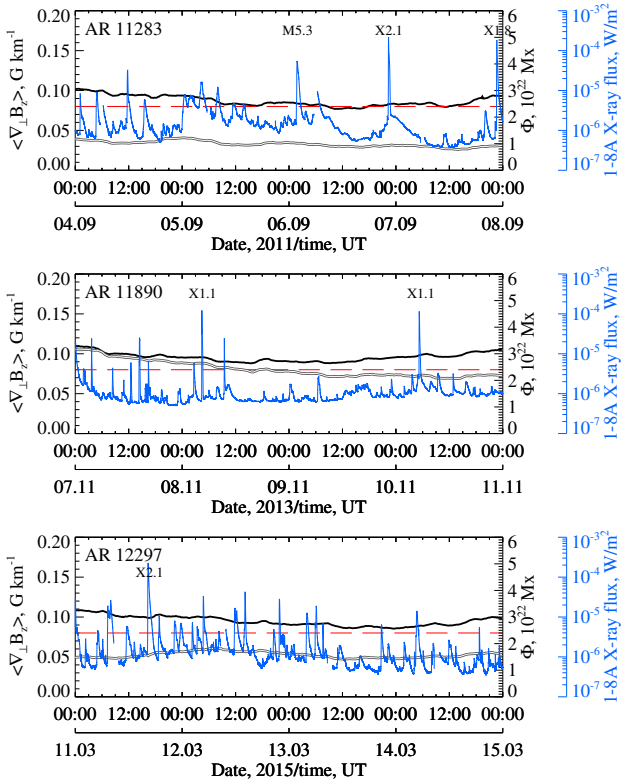

Fig. 4. The same as in Fig. 3 but for three regions with high flare productivity from the analyzed sample. The X-ray classes of the most powerful flares associated with the studied AR are indicated.

(0.120 Gs km^{-1} for NOAA AR 12192) and minimum (0.070 Gs km^{-1} for NOAA AR 11899) values of the parameter $< \overline{\nabla_\perp B_z} >$ differ by a factor of 1.7. Calculating the average value of $< \overline{\nabla_\perp B_z} >$ for the entire sample of ARs, which is 0.092 Gs km^{-1}, the spread of values relative to the average one does not exceed 30%. This can be explained by the fact that regions with low activity often occupy significantly smaller areas and have a weaker magnetic flux compared to regions with high flare productivity. When averaging the parameter, which is the value of $< \nabla_\perp B_z >$, there is a direct link to the AR area since it involves division by the number of pixels the region occupies, resulting in little variation in the numerical values of the parameter $< \nabla_\perp B_z >$ for regions with low and high activity levels. It is likely that future studies in this field will need to use a different parameter that would characterize the longitudinal magnetic field gradient and be independent of the AR area.

2. Despite the insignificant spread in the parameter of $< \nabla_\perp B_z >$, this quantity is systematically greater in ARs with high activity (see the sixth column of Table 1).
3. The conditional boundary of the $< \nabla_\perp B_z >$ value between regions with low activity and flare-productive ARs can be approximately set at the level of 0.08 Gs km^{-1} (minimum values that are characteristic of NOAA AR 11283 with high activity). This level is indicated by the red long-dashed line on the graphs in Figs. 3 and 4.

It would also be extremely interesting to observe the behavior of $< \nabla_\perp B_z >$ in ARs with active magnetic flux emergence during the monitoring time. Two such ARs have been analyzed – NOAA AR 11158 (February 2011) and NOAA AR 12673 (September 2017). In both cases, during the monitoring time, the magnetic flux of the AR increased several times compared to the initial value. The results of analysis are presented in Fig. 4.

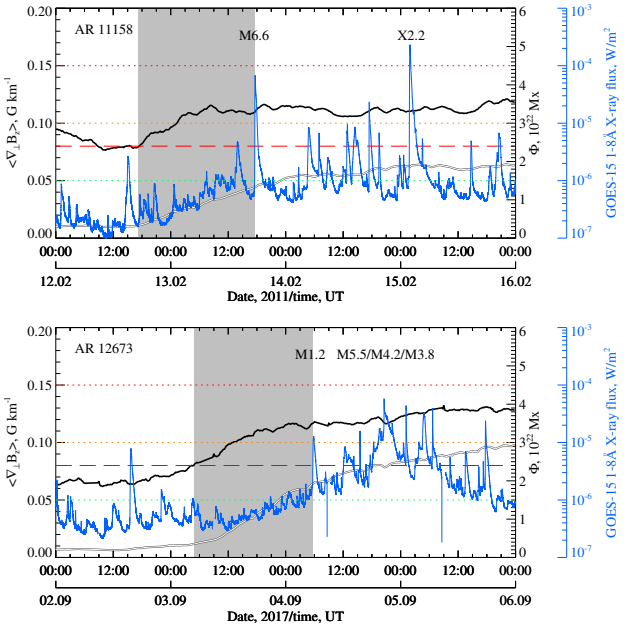

Fig. 5. Dynamics of the magnetic flux (gray double curve), average value of the transverse component of the longitudinal magnetic field gradient $< \nabla_\perp B_z >$ (black curve), and X-ray flux in the 1–8 Å wavelength range at the Earth orbit (blue curve) for NOAA AR 11158 and NOAA AR 12674 with additional magnetic flux emergence. The X-ray classes of the most powerful flares associated with the studied AR are indicated. The gray shading highlights the time interval between the increase in the $< \nabla_\perp B_z >$ value above the critical level (red long-dashed line) and the first flare of X-ray class M.

From the graphs presented in Fig. 5, it can be seen that the value of $< \nabla_\perp B_z >$ also increases by approximately 1.5 to 2 times. The onset of the magnetic field gradient growth coincides with the beginning of magnetic flux increase; however, the gradient growth ceases earlier than the magnetic flux growth. Taking the previously defined critical value of $< \nabla_\perp B_z >$ equal to 0.08 Gs km^{-1}, it can be seen that for ARs with additional magnetic flux emergence, the increase in the $< \nabla_\perp B_z >$ value above the critical level occurs approximately 24 hours before the onset of the first flare events of X-ray class M and higher. Thus, this value can be used as a prognostic parameter indicating a possible increase in the flare activity of the AR, although further research on a larger statistical sample is needed.

3.2 Second approach to calculating the transverse component of the longitudinal magnetic field gradient: features and key findings

The second approach to calculating $\nabla_{\perp}B_z$ can be considered as classical since it is this approach that was used in calculating the longitudinal magnetic field gradients in the first works dedicated to this issue. Given the low spatial resolution, characteristic of early magnetographs, constructing a detailed map of the spatial distribution of the longitudinal magnetic field gradient at a given level was impossible. However, it was possible to measure magnetic fields quite accurately in the most developed sunspots of the AR, as well as to determine distance between them, enabling the calculation of the longitudinal magnetic field gradient between two sunspots using the expression

$$\nabla_{\perp}B_z \equiv \frac{\Delta B_z}{\Delta r} = \frac{\mid B_{zimax} - B_{zjmax} \mid}{\sqrt{(x_i - x_j)^2 + (y_i - y_j)^2}}, \qquad (3)$$

where B_{zimax} and B_{zjmax} are the maximum magnetic field strength in sunspots for which the longitudinal magnetic field gradient is calculated (in Gs); x_i, y_i, x_j, y_j are the coordinates of points with maximum field strength in sunspots; $\sqrt{(x_i - x_j)^2 + (y_i - y_j)^2} \equiv r$ is the distance between sunspots, expressed in kilometers.

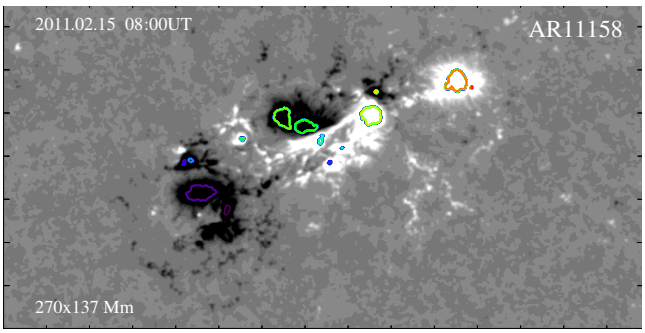

Fig. 6. Individual sunspots with magnetic field strength above 1600 Gs (colored contours) by the example of NOAA AR 11158 from the analyzed sample.

We decided to assess the applicability of this approach in modern contexts using data from high spatial resolution instruments and to compare the obtained results with data from the first approach and from early studies on this topic.

The approach is briefly as follows. Let us consider a certain AR where several isolated sunspots with strong magnetic fields can be distinguished (Fig. 6). Here, a magnetic field is considered strong if the maximum magnetic field strength in the sunspot exceeds 1600 Gs. This value is obtained as follows: magnetic fields that are below the double value, typical for the penumbra of the developed sunspot (800 Gs), are excluded. An alternative approach is to exclude magnetic fields below 1000 Gs (the minimum magnetic field in stable developed sunspots). In that case, besides the main sunspots occupying a significant area, a large number of small structures would also be obtained. Then it would be necessary to exclude small sunspots with an area less than n pixels.

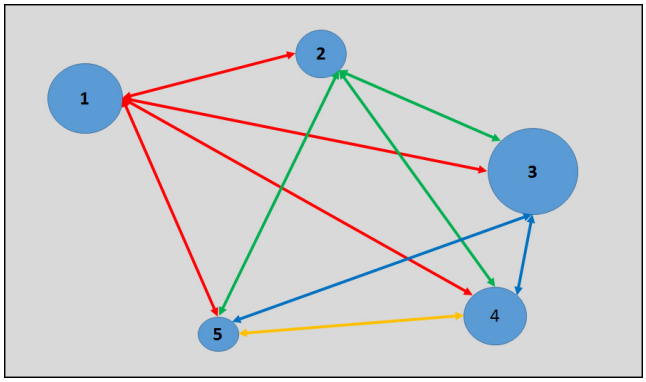

Fig. 7. On calculating the longitudinal magnetic field gradient between individual sunspots in the AR. Schematic representation of the IDL code operation.

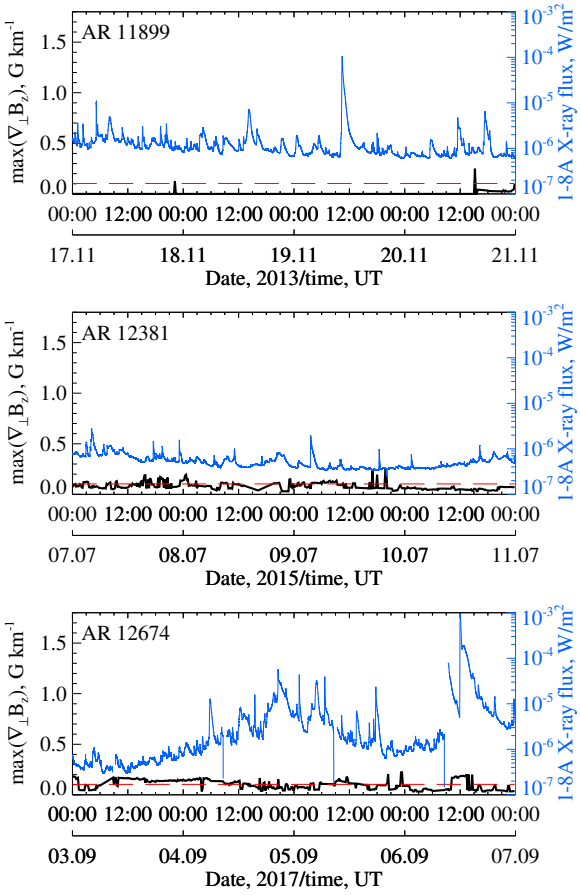

Fig. 8. Dynamics of the maximum value of the transverse component of the longitudinal magnetic field gradient between sunspots in the AR $max(\nabla_{\perp}B_z)$ (black curve) and the X-ray flux in the wavelength range of 1–8 Å at the Earth orbit (blue curve) for three ARs with low flare activity from the analyzed sample. The critical level of the $max(\nabla_{\perp}B_z)$ value is indicated by the red long-dashed line (for more details, see the text).

However, problems emerge regarding the minimum number of pixels that a sunspot should occupy for the necessity of

including it in calculating the magnetic field gradient to arise, as well as how to give reasons for this threshold.

By isolating individual sunspots in the AR, we then proceed directly to calculating the gradients between each pair of sunspots using expression (3). Initially, we calculate the longitudinal magnetic field gradients between the first sunspot and the subsequent ones (red arrows in Fig. 7), then between the second sunspot and the subsequent one (green arrows in Fig. 6), and so on. It is also evident that $\nabla_\perp B_z(1 \rightarrow 2) \equiv \nabla_\perp B_z(2 \rightarrow 1)$, $\nabla_\perp B_z(1 \rightarrow 3) \equiv \nabla_\perp B_z(3 \rightarrow 1)$... Hence, the magnetic field gradient value in such cases is calculated only once.

Upon obtaining the values of $\nabla_\perp B_z$ for all pairs of sunspots for the magnetogram of the studied AR, from a set of values we select only the maximum value (denoted as $max(\nabla_\perp B_z)$) for particular moment in time. Then, we construct a graph showing the temporal variations of $max(\nabla_\perp B_z)$ for the entire AR monitoring time. Examples of such graphs are shown in Fig. 8 (ARs with low activity) and Fig. 9 (ARs with high activity). The X-ray flux in the wavelength range of 1–8 Å at the Earth orbit is also shown (blue curve, data from the GOES-15 spacecraft). The X-ray classes of the most powerful flares (not lower than X5.0) associated with the studied AR during its monitoring time are indicated.

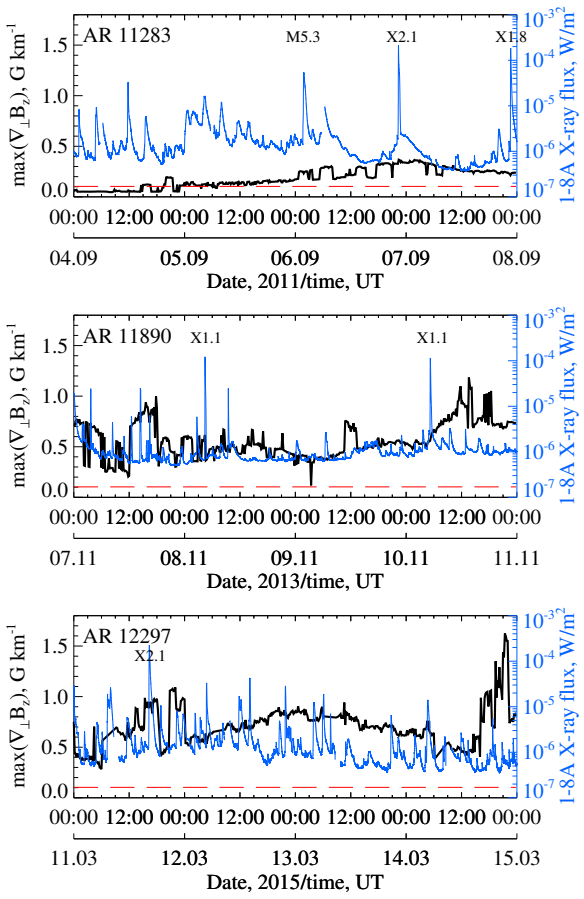

Fig. 9. The same as in Fig. 8 but for three ARs with high flare productivity from the analyzed sample. The X-ray classes of the most powerful flares associated with the studied AR are indicated.

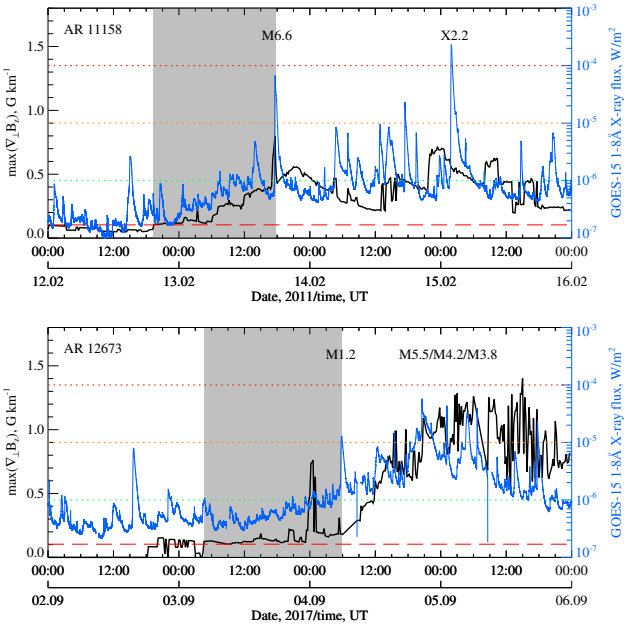

Fig. 10. Dynamics of the maximum value of the transverse component of the longitudinal magnetic field gradient between sunspots in the AR $max(\nabla_\perp B_z)$ (black curve) and the X-ray flux in the wavelength range of 1–8 Å at the Earth orbit (blue curve) for NOAA AR 11158 and NOAA AR 12674 with additional magnetic flux emergence. The X-ray classes of the most powerful flares associated with the studied AR are indicated. The gray shading highlights the time interval between an increase in the $max(\nabla_\perp B_z)$ value above the critical level (red long-dashed line) and the first X-ray flare of class M.

Analyzing the graphs presented in Figs. 8 and 9, the following observations can be made:

1. It is evident from the graphs that the value of $max(\nabla_\perp B_z)$ for ARs with low activity is lower than that for ARs with high flare productivity. This difference is particularly noticeable in the data presented in Table 1, where the last column provides the time-averaged values of $\overline{max(\nabla_\perp B_z)}$ for each region in the studied sample. A conditional boundary between regions with high and low activity can be approximately set at the level of $max(\nabla_\perp B_z)$ at 0.115 Gs km^{-1}.
2. On many graphs, jumps in the value of $max(\nabla_\perp B_z)$ can be observed, sometimes quite significant. These jumps are caused by the evolution of magnetic fields in the AR. Such jumps may be associated either with the decay of one of the two sunspots between which the program previously determined the maximum value of the magnetic field gradient and, accordingly, a switch to another pair of sunspots (in this case, a sudden decrease in the value of $max(\nabla_\perp B_z)$ is observed on the graph) or with the emergence of a new magnetic flux and the formation of a sunspot/sunspots with sufficiently high magnetic field strength near one of the already formed large sunspots in the AR (a sudden increase in the value of $max(\nabla_\perp B_z)$ is observed).

Similar to the application of the first approach to calculating the longitudinal magnetic field gradient, it would be interesting to see how the value of $max(\nabla_\perp B_z)$ behaves in ARs with active magnetic flux emergence. The results are presented in Fig. 10. It can be seen that for both ARs with additional magnetic flux emergence, an increase in the value of $max(\nabla_\perp B_z)$ above a critical value of 0.115 Gs km^{-1} occurs approximately 23–25 hours before the onset of the first flare events of X-ray class M and higher.

3.3 General results

Based on the data presented in the last three columns of Table 1, graphs were constructed showing the dependence between the flare index value and parameters characterizing the transverse component of the longitudinal magnetic field gradient – the averaged over the AR monitoring period values of $< \nabla_\perp B_z >$ and $max(\nabla_\perp B_z)$ (Figs. 11 and 12).

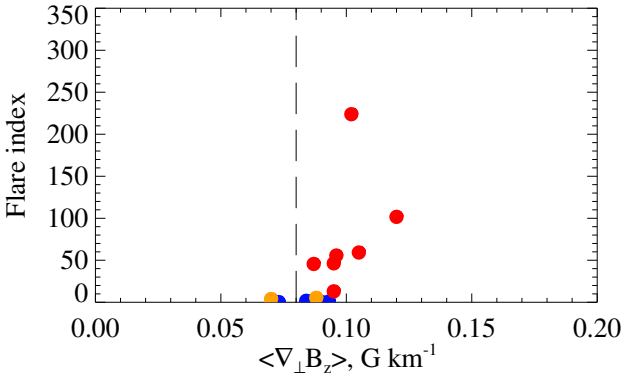

Fig. 11. Graph of the dependence between the average value of the transverse component of the longitudinal magnetic field gradient $< \nabla_\perp B_z >$ and the flare index for the entire sample of ARs. Regions in which flares of X-class X were recorded are marked by red dots; regions with M-class flares, by orange dots; and regions with only flares of X-ray class C, by blue dots. The critical value of the parameter $< \nabla_\perp B_z >$ is indicated by the vertical dash.

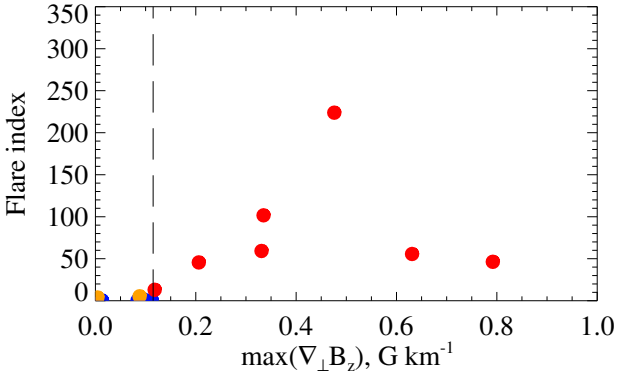

Fig. 12. Graph of the dependence between the maximum value of the transverse component of the longitudinal magnetic field gradient $max(\nabla_\perp B_z)$ between sunspots in ARs and the flare index for the entire analyzed sample of ARs. The same notation as in Fig. 11 is used. The critical value of the parameter $max(\nabla_\perp B_z)$ is marked by the vertical dash.

As can be seen from the graphs presented, no significant correlation is noted: the spread of points is quite great, and there is insufficient data to identify any existing dependence. This result additionally confirms the statement made by many authors that only small part of the energy of non-potential magnetic fields is involved in flare processes. Despite the lack of correlation dependence, the threshold (critical) values of the parameters of the longitudinal magnetic field gradient are evident. This is particularly clear in the relationship between flare index and $max(\nabla_\perp B_z)$, where the separation between regions with low activity and those with and high activity is quite pronounced.

Note that the obtained critical values such as $< \nabla_\perp B_z >= 0.080 - 0.085$ Gs km^{-1} (the first approach to calculating the longitudinal magnetic field gradient) and the parameter $max(\nabla_\perp B_z) = 0.110 - 0.115$ Gs km^{-1} (the second approach) are very close to a value of 0.1 Gs km^{-1} obtained significantly earlier based on quite extensive statistical data (Severnyi, 1960). Naturally, by using the first approach and applying the average value of the longitudinal magnetic field gradient for the analysis over the AR, we should have obtained a value below 0.1 Gs km^{-1}. It was somewhat surprising to obtain a value for the parameter $max(\nabla_\perp B_z)$ that differs little from the value obtained in earlier studies on this topic. This proves the precision of measurements and calculations carried out by Soviet astronomers: despite the absence of high spatial resolution magnetographs, they managed to accurately determine the critical value of the longitudinal magnetic field gradient.

4 Conclusions and discussion

Based on studying the existing approaches to calculating longitudinal magnetic field gradients, determining the values, and analyzing the dynamics of the transverse component of the longitudinal magnetic field gradient ($\nabla_\perp B_z$) for a small sample of 13 active regions with different levels of flare productivity (6 ARs with low, 5 ARs with high flare activity, and two ARs with high activity and additional emergence of the magnetic flux), we can draw the following conclusions:

1. The first approach to calculating the longitudinal magnetic field gradient can only be applied to data acquired with modern high spatial resolution instruments for studying the Sun. This approach involves calculating gradients between neighboring pixels on a magnetogram. This enables the construction of detailed maps of the spatial distribution of the $\nabla_\perp B_z$ value at a given level of the solar atmosphere, identification of the probable locations of occurrence and development of flare processes in ARs.
2. Within the framework of the first approach, it becomes possible to calculate average or integral parameters that can characterize the longitudinal magnetic field gradient. Here, the average transverse component of the longitudinal magnetic field gradient $< \nabla_\perp B_z >$ is chosen as such a parameter. Studying the parameter $< \nabla_\perp B_z >$ in the ARs of the analyzed sample showed that, despite small differences, its value is systematically larger in regions with high flare productivity.
3. Analysis of the dynamics of the parameter $< \nabla_\perp B_z >$ over the monitoring time of the studied regions allowed

revealing a threshold value of this quantity, which is approximately 0.08 Gs km^{-1}, defined as the minimum value for the group of analyzed regions with high activity.
4. The second approach to calculating longitudinal magnetic field gradients (classical) involves calculating the value of $\nabla_\perp B_z$ between individual sunspots in the AR. This approach does not allow for the construction of detailed maps of the distribution of $\nabla_\perp B_z$, but its advantage lies in the ability to apply it to magnetographic data at both high and low spatial resolutions.
5. A parameter characterizing the longitudinal magnetic field gradients within the second approach is $max(\nabla_\perp B_z)$ – the maximum value of the transverse component of the longitudinal magnetic field gradient among pairs of sunspots for a given region and time. Studying the dynamics of the parameter $max(\nabla_\perp B_z)$ has revealed sharp jumps, which are caused by evolutionary changes in magnetic fields in the AR. It has also been found that $max(\nabla_\perp B_z)$ has higher values in ARs with high flare productivity. A critical value of the parameter $max(\nabla_\perp B_z)$ has been identified, which is approximately equal to 0.115 Gs km^{-1}.
6. Studying the ARs with additional emergence of the magnetic flux has shown that the first flares of X-ray class M and higher occur on a timescale of 23–25 hours after exceeding the critical values of $< \nabla_\perp B_z >$ and $max(\nabla_\perp B_z)$.

Note that the characteristic time delays between the increase of longitudinal magnetic field gradients and the first flare events of high X-ray classes for 23–25 hours are obviously of fundamental importance, as many AR parameters undergo changes (sometimes abrupt) approximately 0.5–2 days before the first powerful flares. For example, Smol'kov et al. (2011) report on the emergence of bright neutral sources of microwave radiation in the AR approximately two days before powerful flare events. Abramenko (2016) showed that the slope of the power spectrum in the AR varies and has a local maximum approximately 0.6–1.9 days before the flare. Fursyak et al. (2020) discovered a 20-hour time delay between the increase of the average unsigned density of vertical electric current $< |j_z| >$ above a critical value of 2.7 mA m^{-2} and the first powerful flares in the AR. Several other studies (Pustil'nik, 2001; Strugarek et al., 2014; Gershberg, 2015) also indicate a characteristic time of 0.5–2 days for the transfer of accumulated energy from the photosphere to the corona and producing a critical situation there.

This study is the first in a series of studies aimed at determining the parameters that could characterize the longitudinal magnetic field gradients in the AR and the dynamics that could be compared with the level and temporal variations of flare productivity in the AR. Within the second approach to calculating the magnetic field gradient, the parameter $max(\nabla_\perp B_z)$ was likely chosen successfully, as it allows for easy determination of a threshold value and differentiation between regions of high and low activity. The parameter $< \nabla_\perp B_z >$, selected as the base parameter in the first approach, evidently needs to be replaced with another parameter that is less dependent on the area occupied by the AR. Furthermore, additional research with a statistical dataset is needed to confirm the results obtained here.

This work was supported by the research grant No. 1021051101548-7-1.3.8 "Solar Physics and its Activity on Different Temporal and Spatial Scales".

The author is grateful to the referee for interest and valuable comments that helped to significantly improve this paper.

References

Abramenko V.I., 2005. Astrophys. J., vol. 629, no. 2, pp. 1141–1149.
Abramenko V.I., 2016. Turbulent and multi-fractal nature of solar magnetism (Dr. Sci. thesis). Nauchny. (In Russ.)
Altyntsev A.T., Banin V.G., Kuklin G.V., Tomozov V.M., 1982. Solar Flares, M.: Nauka. (In Russ.)
Avignon Y., Martres M.J., Pick M., 1964. Ann. Astrophys., vol. 27, pp. 23–28.
Babcock H.W., 1953. Astrophys. J., vol. 118, pp. 387–396.
Baranovskii E.A., Stepanov V.E., 1959. Izv. Krymsk. Astrofiz. Observ., vol. 21, pp. 180–189. (In Russ.)
Bobra M.G., Sun X., Hoeksema J.T., Turmon M., Liu Y., et al., 2014. Solar Phys., vol. 289, pp. 3549–3578.
Bruns A.V., Nikulin N.S., Severnyi A.B., 1965. Izv. Krymsk. Astrofiz. Observ., vol. 33, pp. 80–85. (In Russ.)
Caroubalos C., 1964. Ann. Astrophys., vol. 27, pp. 333–388.
Fursyak Yu.A., Abramenko V.I., Kutsenko A.S., 2020. Astrophysics, vol. 63, no. 2, pp. 260–273.
Gershberg R.E., 2015. Solar-Type Activity in Main-Sequence Stars, Simferopol': Antikva. (In Russ.)
Gopasyuk S.I., Ogir' M.B., Severnyi A.B., Shaposhnikova E.F., 1963. Izv. Krymsk. Astrofiz. Observ., vol. 29, pp. 15–67. (In Russ.)
Hale G.E., 1908. Astrophys. J., vol. 28, pp. 315–343.
Houtgast J., van Sluiters A., 1948. Bull. Astron. Inst. Netherl., vol. 10, pp. 325–333.
Ioshpa B.A., Mogilevskii E.I., 1965. Soln. aktivnost', no. 2, pp. 118–130. (In Russ.)
Ioshpa B.A., Obridko V.N., 1965. Soln. dannye, no. 3, pp. 54–58. (In Russ.)
Ikhsanov R.N., Platonov Yu.P., 1967. Solnechnye dannye, no. 11, pp. 78–89. (In Russ.)
Kosugi T., Matsuzaki K., Sakao T., Shimizu T., Sone Y., et al., 2007. Solar Phys., vol. 243, pp. 3–17.
Kotov V.A., 1970. Izv. Krymsk. Astrofiz. Observ., vol. 41–42, pp. 67–88. (In Russ.)
Kuznetsov D.A., Kuklin G.V., Stepanov V.E., 1966. Rezul'taty nablyudenii i issledovanii v period MGSS, iss. 1, pp. 80–87. (In Russ.)
Lee R.H., Rust R.M., Zirin H., 1965. Applied Optics IP, vol. 4, pp. 1081–1084.
Leroy J.L., 1962. Ann. Astrophys., vol. 25, pp. 127–165.
Livingston W.C., 1968. Astrophys. J., vol. 153, pp. 929–942.
Nikulin N.S., 1967. Izv. Krymsk. Astrofiz. Observ., vol. 36, pp. 76–86. (In Russ.)
Nikulin N.S., Severnyi A.B., Stepanov V.E., 1958. Izv. Krymsk. Astrofiz. Observ., vol. 19, pp. 3–19. (In Russ.)
Pesnell W.D., Thompson B.J., Chamberlin P.C., 2012. Solar Phys., vol. 275, pp. 3–15.
Pustil'nik L., 2001. Proc. of the 27th International Cosmic Ray Conference, pp. 3250–3253.
Severnyi A.B., 1956. Astron. zhurn., iss. 33, pp. 74–79. (In Russ.)

Severnyi A.B., 1957. Astron. zhurn., iss. 34, pp. 684–693. (In Russ.)
Severnyi A.B., 1958. Izv. Krymsk. Astrofiz. Observ., vol. 20, pp. 22–51. (In Russ.)
Severnyi A.B., 1960. Izv. Krymsk. Astrofiz. Observ., vol. 22, pp. 12–41. (In Russ.)
Severnyi A.B., 1965. Izv. Krymsk. Astrofiz. Observ., vol. 33, pp. 3–33. (In Russ.)
Severnyi A.B., 1988. Some Problems of Solar Physics, M.: Nauka. (In Russ.)
Severny A.B., Stepanyan N.N., Steshenko N.V., 1979. NOAA Solar-Terrest. Prediction Proc., vol. 1, pp. 72–88.

Smol'kov G.Ya., Maksimov V.P., Prosovetskii D.V., Uralov A.M., Bakunina I.A., et al., 2011. Solnechno-zemnaya fizika, iss. 18, pp. 74–78. (In Russ.)

Scherrer P.H., Schou J., Bush R.I., Kosovichev A.G., Bogart R.S., et al., 2012. Solar Phys., vol. 275, pp. 207–227.

Strugarek A., Charbonneau P., Joseph R., Pirot D., 2014. Solar Phys., vol. 289, pp. 2993–3015.

Zvereva A.M., Severnyi A.B., 1970. Izv. Krymsk. Astrofiz. Observ., vol. 41–42, pp. 97–157. (In Russ.)